Si Hybrid Solar Cells with up to 13% Efficiency *via* Concurrent Improvement in Optical and Electrical Properties by Employing Graphene Quantum Dots

Meng-Lin Tsai,[1,2] Wan-Rou Wei,[1] Libin Tang,[3] Hung-Chih Chang,[1] Shih-Hsiang Tai,[1] Po-Kang Yang,[1] Shu Ping Lau,[3] Lih-Juann Chen,[2,*] and Jr-Hau He[1,*]

[1]*Institute of Photonics and Optoelectronics and Department of Electrical Engineering, National Taiwan University, Taipei 10617, Taiwan, ROC*

[2]*Department of Materials Science and Engineering, National Tsing Hua University, Hsinchu 30013, Taiwan, ROC*

[3]*Department of Applied Physics, The Hong Kong Polytechnic University, Hong Kong SAR*

[*]Corresponding author e-mail: jhhe@cc.ee.ntu.edu.tw; ljchen@mx.nthu.edu.tw

Abstract

By employing graphene quantum dots (GQDs) in PEDOT:PSS, we have achieved the efficiency of 13.22% in Si/PEDOT:PSS hybrid solar cells. The efficiency enhancement is based on concurrent improvement in optical and electrical properties by the photon downconversion process and the improved conductivity of PEDOT:PSS *via* appropriate incorporation of GQDs. After introducing GQDs into PEDOT:PSS, the short circuit current and the fill factor of hybrid cells are increased from 32.11 to 36.26 mA/cm^2 and 62.85% to 63.87%, respectively. The organic-inorganic hybrid solar cell obtained herein holds the promise for developing photon-managing, low-cost, and highly efficient photovoltaic devices.

Photon management strategies using microstructures or nanostructures to manipulate the light have been widely used for various optical devices such as photodetectors,[1,2] light-emitting diodes,[3,4] and photovoltaics.[5-19] As for photovoltaics, it has been reported that nanostructuring and/or microstructuring the surface of solar cells can harvest more light and thus enhance the absorption of the active layer.[5-19] Furthermore, in order to achieve high-efficiency photovoltaic devices, various techniques have been provided to improve not only optical characteristics but also electrical properties. For improving electrical properties, surface engineering methods such as chemical treatment procedures have been applied to improve the surface quality, reduce dangling bonds, and provide additional built-in electric field to induce carrier separation effectively at the interface.[8,9] Concurrent improvement in optical and electrical properties would greatly improve open-circuit voltage (V_{OC}), short-circuit current density (J_{SC}), and fill factor (*FF*) of the solar device, leading to a higher power conversion efficiency (*PCE*).[8,9,18]

Si-based solar cells have dominated the commercial photovoltaic market in the past decades, due to highly abundant Si materials, acceptable *PCE*s, and mature Si semiconductor technologies. However, the cost to produce electricity per watt is still high as compared to traditional energies.[20] Therefore, how to improve the “cost effectiveness” of Si-based solar energy becomes an important task both in industrial development and scientific research. As most of the cost in fabricating Si-based solar cells comes from conventional high temperature procedures such as doping and ion implantation processes, Si-organic based hybrid heterojunction solar cells fabricated at low temperatures have become an emerging technology to effectively reduce the fabrication cost.[8,10-14]

Si-organic based hybrid solar cells have been developed to adopt both the advantages of the inorganic substance and Si to obtain a high *PCE* at a relatively low

production cost. *PCE*s over 10% have been successfully reached in such devices by either enhancing the optical or the electrical properties of the cells. For example, the Zonyl addition to poly(3,4-ethylene-dioxythiophene):polystyrenesulfonate (PEDOT:PSS) significantly improves electrical properties *via* facilitating the adhesion on hydrophobic Si wafers, achieving the *PCE* of 11.34%.[13] Moreover, much effort to suppress the light reflection and enhance the photogenerated carrier collection efficiency has been made for the purpose of optical and electrical concurrent improvement *via* nanostructuring cells. The approaches are based on considering theoretically superior light trapping ability, significant increase in the p-n junction areas, and shortening carrier diffusion distance.[10,11,14,15,17,18] However, trapping light as much as possible simply by increasing the aspect-ratio of Si nanowires usually comes with a large shunt leakage across the cells due to the excessive junction, surface recombination losses, and unconformal deposition of the metal electrodes over high aspect-ratio Si nanostructure surfaces, yielding an unsatisfactory *PCE* of the cell. Recently, a creditable attempt has been successful to achieve a high *PCE* (11.48%) of hybrid solar cells by employing hierarchical structures providing efficient charge separation/transport *via* increasing junction areas without sacrificing the optical absorption.[8] However, there is still a large gap in efficiency between hybrid and conventional Si solar cells, impeding their development to becoming cost-effective devices.

Graphene has received much attention in a wide range of fields due to its high mobility. However, the lack of bandgap limits its potential in the practical applications in semiconductor devices. Various efforts have been devoted to opening its bandgap, which requires additional doping processes and becomes complicated and costly. Graphene quantum dots (GQDs) exhibit unique semiconducting behavior and become a newly emerging material for optoelectronic applications.[21,22] The bandgap of GQDs

has also been reported to be dependent on their chemical functionality.[22] One of the most interesting features of GQDs, however, is the photon downconversion property, which is the ability to absorb photons in shorter wavelength regions and then emit photons in longer wavelength regions. This phenomenon has previously been observed in rare earth materials and some II-VI semiconducting nanoparticles.[16] Employing these photon downconverters which absorb light in the ultraviolet region and emit light in the visible region could possibly exceed the Shockley–Queisser limit, the maximum theoretical *PCE* of a solar cell.[23] In addition to their distinguished optical properties, GQDs can further enhance the conductivity of the organic layer due to the inherent high mobility of graphene to improve electrical properties of the device. The superior solubility of GQDs in aqueous solution can also be integrated well with organic solution and becomes more suitable, as compared with typical layer-like 2D materials, to uniformly deposit on a variety of surface structures such as micropyramids or nanowires.

In this study, the introduction of GQDs to PEDOT:PSS for PEDOT:PSS/Si organic-inorganic hybrid solar cells leads to the increase of J_{SC} from 32.11 mA/cm^2 to 36.26 mA/cm^2 and *FF* from 62.85% to 63.87% due to combined effects of photon downconversion and improved conductivity of the PEDOT:PSS layer by GQDs. The concurrent improvement in optical and electrical properties due to the introduction of GQDs gives rise to a world-record high *PCE* of 13.22% among all the reported Si/organic hybrid solar cells. The realization of high-efficiency hybrid solar cells demonstrated here makes GQDs attractive for large-area and cost-effective cell production.

Figure 1a shows the transmission electron microscopy (TEM) image of the GQDs assembled on carbon film-coated Cu grids. The high-resolution TEM (HRTEM) image in the inset of Figure 1a reveals the microstructure of a single GQD, exhibiting

0.246-nm fringes corresponding to the *d* spacing between graphene layers.[24] From the atomic force microscopy (AFM) image in Figure 1b, the size of the GQDs can be quantitatively characterized. In the figure, the diameter of the GQDs along the blue dashed line is around 2.9 nm, which corresponds to ~12 layers of graphene in each QD. Figure 1c is the size distribution of the GQDs measured in TEM images. It is shown that the average size of GQDs is 3.2 nm with the full-width-at-half-maximum (FWHM) of the fitted Gaussian curve of 0.5 nm, demonstrating that the size of GQDs can be well-controlled. Detailed preparation procedures of these water-soluble GQDs are described in the Supporting Information.

The fabrication process of GQD-modified PEDOT:PSS/Si hybrid solar cells was carried out according to the procedure shown in Figure 2. The micropyramid arrays were fabricated on the top of the n-type Si substrate *via* an electrodeless chemical etching process.[9,19] GQDs with various concentrations were then added to the PEDOT:PSS solution prior to the spin-coating process. The PEDOT:PSS solution is composed of PEDOT:PSS (PH 500 from Clevios) with 5 wt% of dimethyl sulfoxide (DMSO from Sigma-Aldrich) and 0.1 wt% of Triton X surfactant (Triton X-100 from Sigma-Aldrich). The PEDOT:PSS solution with GQDs was spin-coated on the Si substrate, followed by an annealing process at 165 °C for 10 min. Finally, the Ag top finger electrode and the Al back electrode were thermally evaporated on the sample. Detailed device fabrication processes can be seen in the Supporting Information.

To verify the photon downconversion behavior of GQDs, we have performed the photoluminescence (PL) and photoluminescence excitation (PLE) spectroscopy measurements. As shown in Figure 3a, the PL spectrum was measured under the excitation wavelength of 370 nm. The broadband emission with the peak at 451 nm is similar to the previous studies.[21,22] The PLE spectrum measured at the emission peak of PL (451 nm) shows an excitation peak at 373 nm. From the above spectra, it is

evident that photons can be downconverted from the ultraviolet (UV) region to the visible region by the GQDs.

In addition, the absorption spectra of the PEDOT:PSS layers with various GQD concentrations have been measured to characterize the light absorption properties. Figure 3b shows the absorbance spectra of PEDOT:PSS layers with and without GQDs on glass substrates. For aiding to further assess the absorption characteristics of the GQDs, we define the absorption enhancement as the absorbance ratio of the PEDOT:PSS layer with GQDs and the PEDOT:PSS layer without GQDs multiplied by 100% (Figure 3c). One can see that PEDOT:PSS layers with GQDs exhibit vastly enhanced light absorption at the near UV region, which is consistent with the results shown in Figure 3a.

After sequential device fabrication processes, current density-voltage (*J*-*V*) characteristics of hybrid devices with various concentrations of GQDs on Si substrates were measured under the AM 1.5G illumination, as shown in Figure S1. The measured photovoltaic parameters are summarized in Table S1. It is shown that higher concentration of GQDs leads to higher J_{SC}, indicating more photons being absorbed and downconverted in PEDOT:PSS layers. The device with 0.5 wt% of GQDs shows the highest *FF*, leading to the highest *PCE* of 10.88%. The decrease in *FF* with GQD concentration higher than 0.5 wt% could be attributed to the increased recombination events induced with excess amount of GQDs, which will be discussed later.

Despite the efforts being accomplished in enhancing the light harvesting ability and the carrier separation efficiency at the interface of organic and inorganic materials, we made the effort to improve the rear contact quality for reducing the back surface recombination and the series resistance of the device. The highly doped layer creates an ohmic contact and forms a built-in electric field between Si and the back electrode

to reduce the recombination rate at the back surface, resulting in higher V_{OC} and J_{SC}. Accordingly, to further boost the performance of the hybrid solar cells, the devices were fabricated with back surface field-treated substrates. The back surface field in Si is formed by a heavily doped layer through a thermal diffusion of $POCl_3$. As shown in Figure 4a and Table 1, with improved ohmic contact, induced built-in electric potential, and reduced recombination sites at the junction between Si and rear contacts, V_{OC} and J_{SC} can be improved significantly. Consistent with the results above, the device with 0.5 wt% of QDs shows an efficiency of 13.22%, which is the highest among all reported Si/organic hybrid devices (Table S2). In Table 1, the photovoltaic parameters are averaged over three different devices for each condition to verify the results. The high temperature rear doping process is carried out at the Si substrate processing stage without affecting the subsequent low-temperature hybrid cell fabrication procedure.[25] Recently, rear contact engineering techniques at low temperatures for lowering thermal budget have been reported and may be applicable for next-generation hybrid cell devices.[26]

The external quantum efficiency (EQE) spectra of the devices with 0.5 wt% and without GQDs and the EQE enhancement are shown in Figure 4b and Figure 4c, respectively. The EQE enhancement is defined as the EQE of the device with 0.5 wt% GQDs divided by that of the device without GQDs. One can see that in addition to the broadband EQE enhancement in the visible light region, there is a peak of EQE enhancement at 400 nm. The peak of EQE enhancement at 400 nm is consistent with the absorption and the PLE spectrum of the GQDs, which can be attributed to the photon downconversion behavior. For Si-based devices, most of the UV radiation produces photogenerated carriers near the surface. The photogenerated carriers could easily recombine in the presence of surface defects, leading to poor quantum efficiency at UV regions.[2] With the addition of GQDs in PEDOT:PSS layers, part of

the UV radiation can be well converted to visible light *via* the downconversion behavior and reaches the depletion region of the device for photon absortption and photoexcited carrier separation due to the built-in electric field, leading to largely increased quantum efficiency at UV regions. Meanwhile, the slight broadband enhancement from 500 nm up to 1000 nm corresponds to the enhanced carrier collection efficiency due to the improved conductivity by employing GQDs, which will be discussed below.

In Figure 4a and Table 1, it is revealed that devices with GQD concentrations above 0.5 wt% show noticeable decrease in J_{SC}, *FF*, and *PCE*. To gain insight into the phenomenon, we have performed the effective minority carrier lifetime measurement using the quasi-steady-state photoconductance technique to evaluate surface/interface defects. As shown in Figure 5a, devices without GQDs and with 0.1 and 0.5 wt% GQDs show similar carrier lifetimes, whereas the device with 1 wt% GQDs shows an obvious decrease in the minority carrier lifetime. The relatively short carrier lifetime reveals that a more drastic carrier recombination event occurs in the device with excess amount of GQDs. This is possibly due to the aggregation of GQDs, forming carrier-trapping centers and preventing carriers being collected. We have measured the sheet resistance of the PEDOT:PSS layers with different concentrations of GQDs to understand the photovoltaic parameter trend shown in Table 1. It is seen in Figure 5b that the sheet resistance of the PEDOT:PSS layer exhibits the minimum at 0.5 wt% and becomes higher at 1 wt%, leading to increased series resistance and reduced *FF* of the device. Accordingly, improved carrier collection efficiency due to the improved conductivity by employing GQDs with an appropriate concentration leads to the broadband enhancement from 500 nm to 1000 nm. We note that further improvement in the purity of GQD solution and the understanding of carrier recombination behavior at the interface of GQDs and PEDOT:PSS should be studied for optimizing

the performance of the hybrid cell, which is under investigation.

Conclusions

We have successfully fabricated Si/PEDOT:PSS hybrid solar cells with an efficiency up to 13.22% by concurrent improvement in optical and electrical properties *via* the downconversion effect and enhanced conductivity of PEDOT:PSS due to introduction of GQDs. The low-cost, photon-managing, and high-performance device design based on low-temperature solution processes holds the promise for more cost-effective Si-based optical devices.

Figure captions

Figure 1. (a) TEM and HRTEM (inset) images of GQDs. (b) AFM image of GQDs. (c) The diameter distribution of the GQDs measured in TEM images. The blue line in (c) is the Gaussian fitting curve.

Figure 2. Fabrication process of PEDOT:PSS/Si hybrid solar cells with GQDs.

Figure 3. (a) PLE (left) and PL (right) spectra of GQDs. (b) Absorbance spectra of PEDOT:PSS layers without GQDs and with 0.1 wt%, 0.5 wt%, and 1 wt% of GQDs on glass substrates. (c) Absorption enhancement of PEDOT:PSS layers with 0.1 wt%, 0.5 wt%, and 1 wt% of GQDs on glass substrates.

Figure 4. (a) *J-V* characteristics of PEDOT:PSS/Si hybrid solar cells without GQDs and with 0.1, 0.3, 0.5, 0.7, and 1 wt% of GQDs. (b) EQE spectra of PEDOT:PSS/Si hybrid solar cells without GQDs and with 0.5 wt% of GQDs. (c) EQE enhancement of PEDOT:PSS/Si hybrid solar cells with 0.5 wt% as compared to cells without GQDs.

Figure 5. (a) Minority carrier lifetime of cells and (b) sheet resistivity of PEDOT:PSS layer with various concentrations of GQDs.

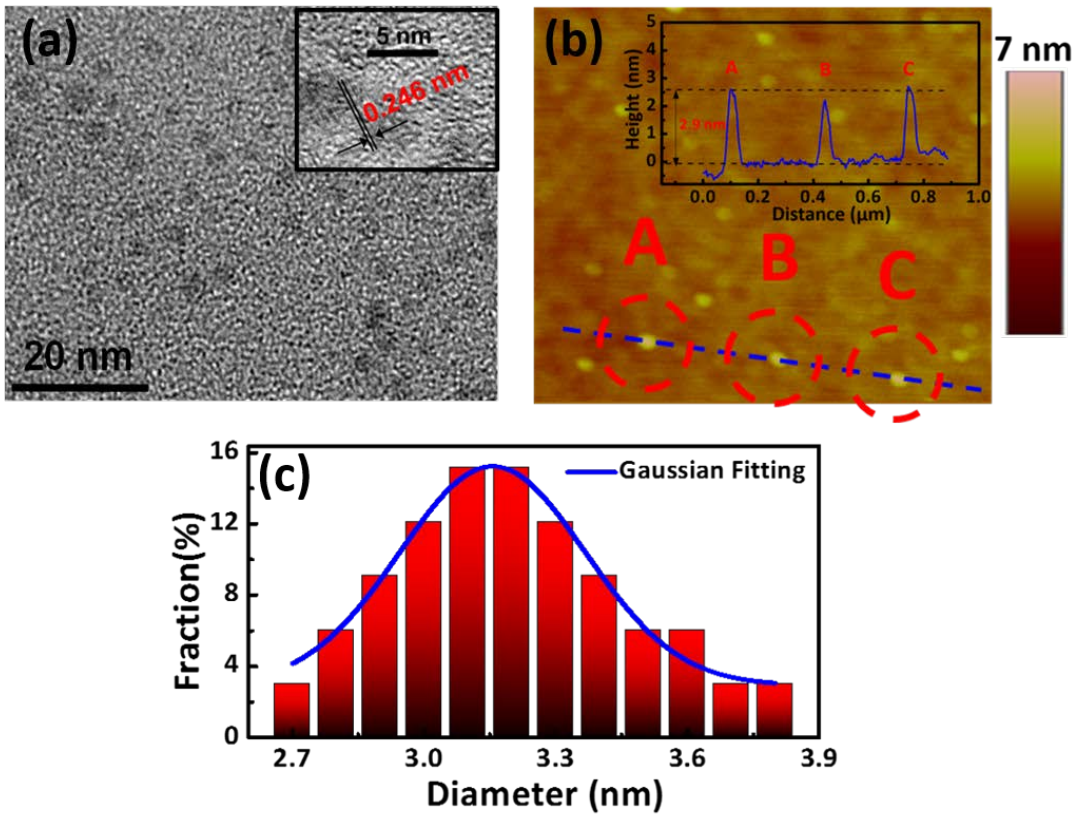
(a)
5 nm
0.246 nm
20 nm
(b)
Height (nm)
A
B
C
2.9 nm
Distance (μm)
7 nm
(c)
Gaussian Fitting
Fraction(%)
Diameter (nm)

Figure 1

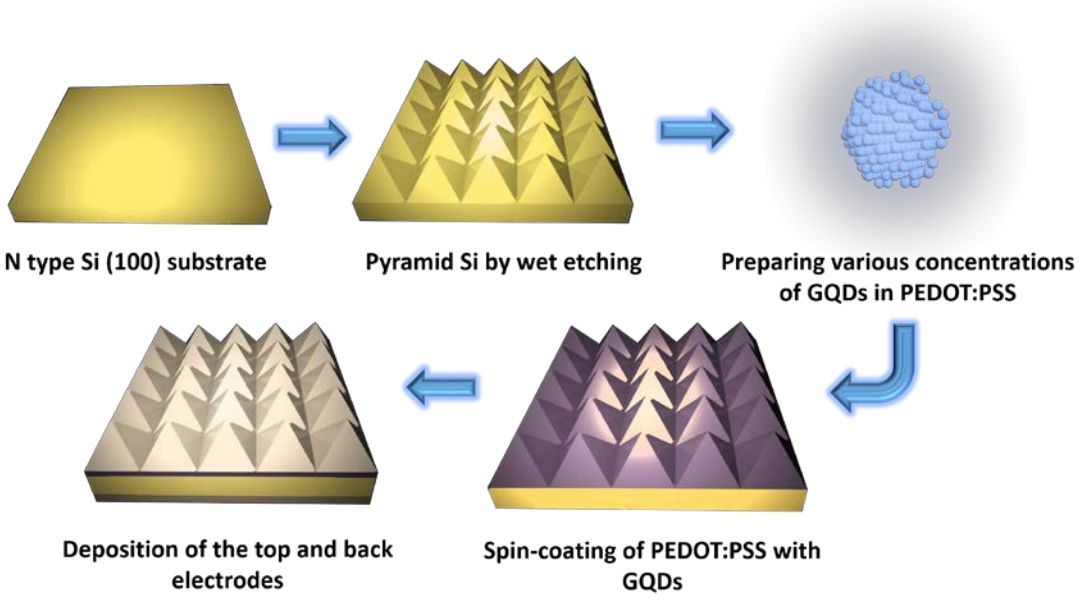
N type Si (100) substrate
Pyramid Si by wet etching
Preparing various concentrations of GQDs in PEDOT:PSS
Spin-coating of PEDOT:PSS with GQDs
Deposition of the top and back electrodes

Figure 2

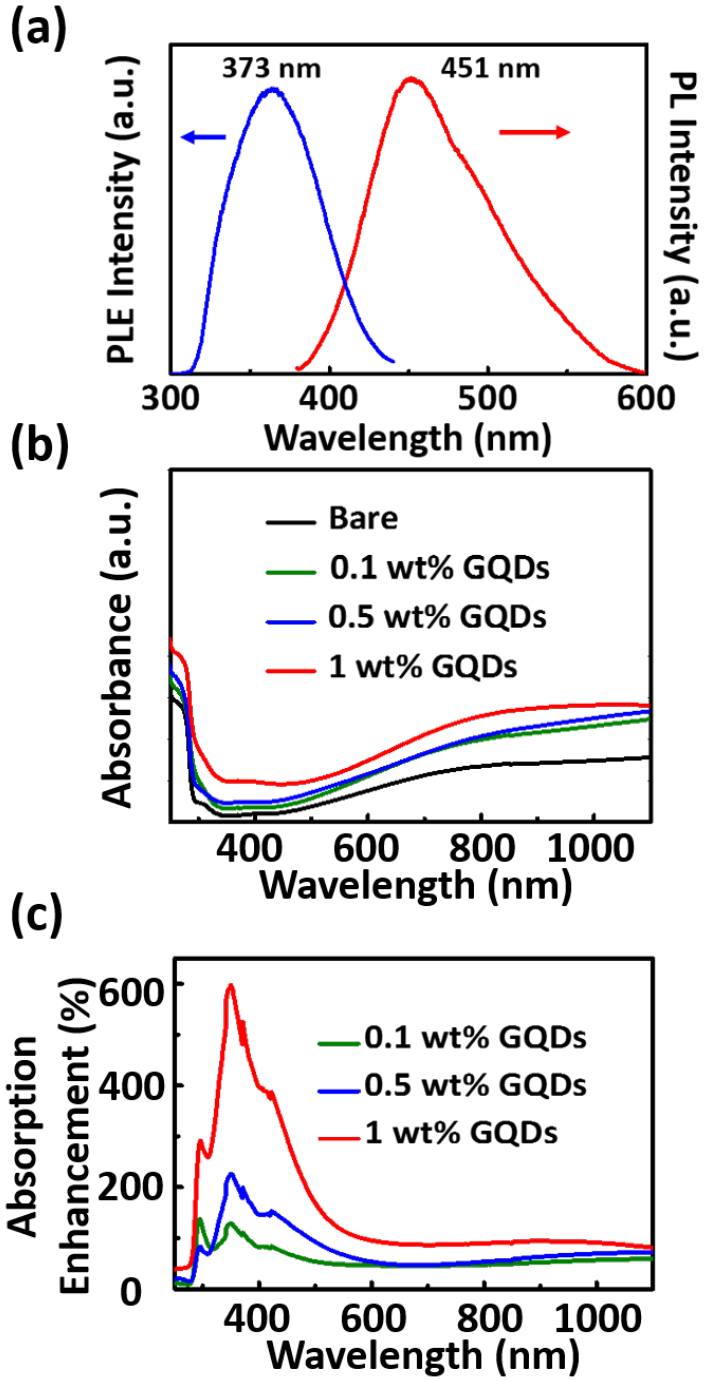
(a)
373 nm
451 nm
PLE Intensity (a.u.)
PL Intensity (a.u.)
300
400
500
600
Wavelength (nm)
(b)
Absorbance (a.u.)
Bare
0.1 wt% GQDs
0.5 wt% GQDs
1 wt% GQDs
400
600
800
1000
Wavelength (nm)
(c)
Absorption Enhancement (%)
600
400
200
0
0.1 wt% GQDs
0.5 wt% GQDs
1 wt% GQDs
400
600
800
1000
Wavelength (nm)

Figure 3

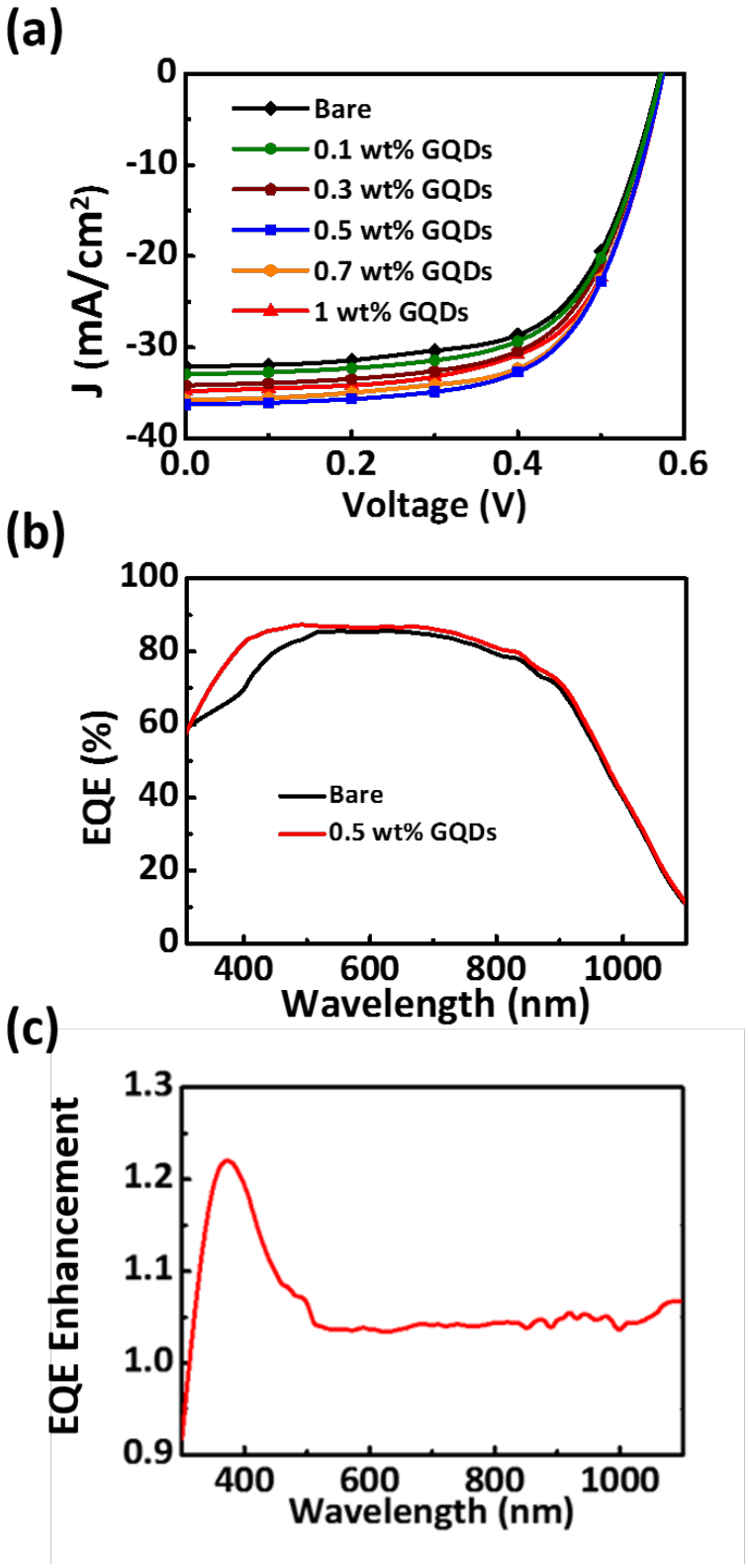
(a)
J (mA/cm²)
Voltage (V)
Bare
0.1 wt% GQDs
0.3 wt% GQDs
0.5 wt% GQDs
0.7 wt% GQDs
1 wt% GQDs
(b)
EQE (%)
Wavelength (nm)
Bare
0.5 wt% GQDs
(c)
EQE Enhancement
Wavelength (nm)

Figure 4

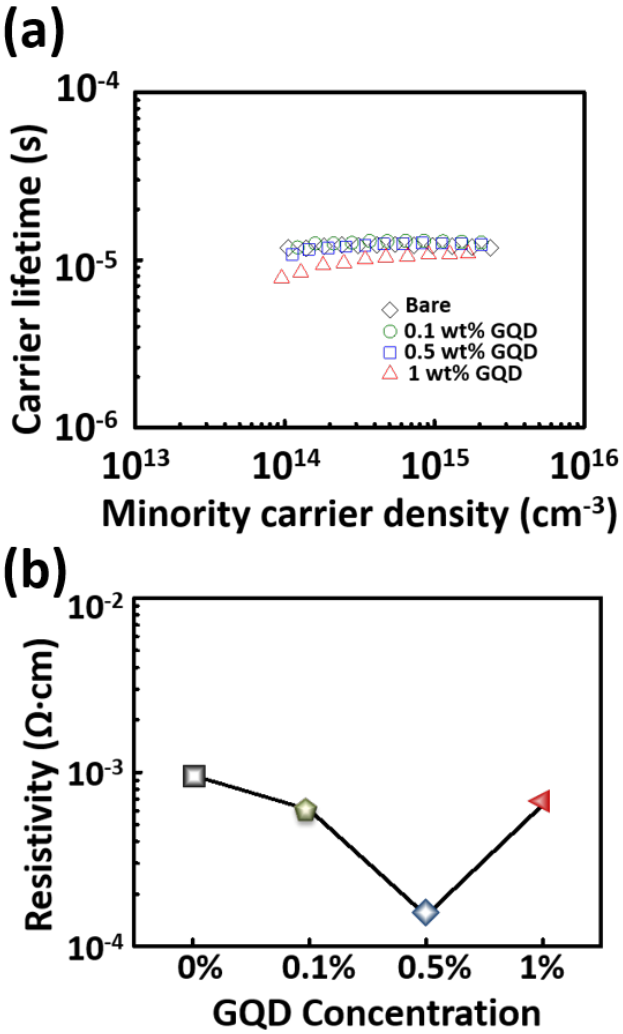
(a)
Carrier lifetime (s)
10-4
10-5
10-6
Bare
0.1 wt% GQD
0.5 wt% GQD
1 wt% GQD
10^13
10^14
10^15
10^16
Minority carrier density (cm-3)
(b)
Resistivity (Ω·cm)
10-2
10-3
10-4
0%
0.1%
0.5%
1%
GQD Concentration

Figure 5

Table 1. Photovoltaic parameters[a] of PEDOT:PSS/Si hybrid solar cells with various concentrations of GQDs.

GQDs	V_{OC} (V)	J_{SC} (mA/cm^2)	*FF* (%)	*PCE* (%)	R_s (Ω·cm^2)	R_{sh} (Ω·cm^2)
0 wt%	**0.57**	**32.11**	**62.85**	**11.50**	3.14	194.10
	0.571 ± 0.002	32.05 ± 0.07	62.49 ± 0.34	11.42 ± 0.04		
0.1 wt%	**0.57**	**32.92**	**63.39**	**11.89**	3.08	231.51
	0.572 ± 0.001	32.69 ± 0.23	63.11 ± 0.27	11.80 ± 0.13		
0.3 wt%	**0.57**	**34.16**	**63.70**	**12.42**	2.94	396.89
	0.569 ± 0.002	33.98 ± 0.16	63.41 ± 0.27	12.30 ± 0.09		
0.5 wt%	**0.57**	**36.26**	**63.87**	**13.22**	2.84	509.27
	0.571 ± 0.002	35.86 ± 0.35	63.67 ± 0.19	13.01 ± 0.13		
0.7 wt%	**0.57**	**35.77**	**63.77**	**13.01**	2.88	437.10
	0.570 ± 0.001	35.24 ± 0.47	63.55 ± 0.19	12.77 ± 0.20		
1 wt%	**0.57**	**34.77**	**62.25**	**12.41**	2.91	372.87
	0.571 ± 0.002	34.59 ± 0.20	62.11 ± 0.13	12.27 ± 0.09		

[a] Data and statistics are based on the average of three different devices. Bold numbers are the values of device with the highest efficiency.

References

(1) Hsu, C. Y.; Lien, D. H.; Lu, S. Y.; Chen, C. Y.; Kang, C. F.; Chueh, Y. L.; Hsu, W. K.; He, J. H. Supersensitive, Ultrafast, and Broad-Band Light-Harvesting Scheme Employing Carbon Nanotube/TiO_2 Core-Shell Nanowire Geometry. *ACS Nano* **2012**, *6*, 6687-6692.

(2) Tsai, D. S.; Lin, C. A.; Lien, W. C.; Chang, H. C.; Wang, Y. L.; He, J. H. Ultra-High-Responsivity Broadband Detection of Si Metal-Semiconductor-Metal Schottky Photodetectors Improved by ZnO Nanorod Arrays. *ACS Nano* **2011**, *5*, 7748-7753.

(3) Hsiao, Y. H.; Chen, C. Y.; Huang, L. C.; Lin, G. J.; Lien, D. H.; Huang, J. J.; He, J. H. Light Extraction Enhancement with Radiation Pattern Shaping of Light Emitting Diodes by Waveguiding Nanorods with Impedance-Matching Tips. *Nanoscale* **2014**, *6*, 2624-2628.

(4) Ho, C. H.; Lien, D. H.; Hsiao, Y. H.; Tsai, M. S.; Chang, D.; Lai, K. Y.; Sun, C. C.; He, J. H. Enhanced Light-Extraction from Hierarchical Surfaces Consisting of p-GaN Microdomes and SiO_2 Nanorods for GaN-Based Light-Emitting Diodes. *Appl. Phys. Lett.* **2013**, *103*, 161104.

(5) Wang, H. P.; Lai, K. Y.; Lin, Y. R.; Lin, C. A.; He, J. H. Periodic Si Nanopillar Arrays Fabricated by Colloidal Lithography and Catalytic Etching for Broadband and Omnidirectional Elimination of Fresnel Reflection. *Langmuir* **2010**, *26*, 12855-12858.

(6) Lin, Y. R.; Lai, K. Y.; Wang, H. P.; He, J. H. Slope-Tunable Si Nanorod Arrays with Enhanced Antireflection and Self-Cleaning Properties. *Nanoscale* **2010**, *2*, 2765-2768.

(7) Lin, Y. R.; Wang, H. P.; Lin, C. A.; He, J. H. Surface Profile-Controlled Close-Packed Si Nanorod Arrays for Self-Cleaning Antireflection Coatings. *J. Appl. Phys.* **2009**, *106*, 114310.

(8) Wei, W. R.; Tsai, M. L.; Ho, S. T.; Tai, S. H.; Ho, C. R.; Tsai, S. H.; Liu, C. W.; Chung, R. J.; He J. H. Above-11%-Efficiency Organic-Inorganic Hybrid Solar Cells with Omnidirectional Harvesting Characteristics by Employing Hierarchical Photon Trapping Structures. *Nano Lett.* **2013**, *13*, 3658-3663.

(9) Wang, H. P.; Lin, T. Y.; Hsu, C. W.; Tsai, M. L.; Huang, C. H.; Wei, W. R.; Huang, M. Y.; Chien, Y. J.; Yang, P. C.; Liu, C. W.; Chou, L. J.; He, J. H. Realizing High-Efficiency Omnidirectional n-Type Si Solar Cells via the Hierarchical Architecture Concept with Radial Junctions. *ACS Nano* **2013**, *7*, 9325-9335.

(10) Jeong, S.; Garnett, E. C.; Wang, S.; Yu, Z.; Fan, S.; Brongersma, M. L.; McGehee, M. D.; Cui, Y. Hybrid Silicon Nanocone-Polymer Solar Cells. *Nano Lett.* **2012**, *12*, 2971-2976.

(11) Tsai, S. H.; Chang, H. C.; Wang, H. H.; Chen, S. Y.; Lin, C. A.; Chen, S. A.; Chueh, Y. L.; He, J. H. Significant Efficiency Enhancement of Hybrid Solar Cells Using Core-Shell Nanowire Geometry for Energy Harvesting. *ACS Nano* **2011**, *5*, 9501-9510.

(12) Yu, P.; Tsai, C. Y.; Chang, J. K.; Lai, C. C.; Chen, P. H.; Lai, Y. C.; Tsai, P. T.; Li, M. C.; Pan, H. T. Huang, Y. Y.; Wu, C. I.; Chueh, Y. L.; Chen, S. W.; Du, C. H.; Horng, S. F.; Meng, H. F. 13% Efficiency Hybrid Organic/Silicon-Nanowire Heterojunction Solar Cell via Interface Engineering. *ACS Nano* **2013**, *7*, 10780-10787.

(13) Liu, Q.; Ono, M.; Tang, Z.; Ishikawa, R.; Ueno, K.; Shirai, H. High Efficient Crystalline Silicon/Zonyl Fluorosurfactant-Treated Organic Heterojunction Solar Cells. *Appl. Phys. Lett.* **2012**, *100*, 183901.

(14) Yang, Y.; Zhang, H. L.; Zhu, G.; Lee, S.; Lin, Z. H.; Wang, Z. L. Flexible Hybrid Energy Cell for Simultaneously Harvesting Thermal, Mechanical, and Solar Energies. *ACS Nano* **2013**, *7*, 785-790.

(15) Fan, Z.; Kapadia, R.; Leu, P. W.; Zhang, X.; Chueh, Y. L.; Takei, K.; Yu, K.; Jamshidi, A.; Rathore, A.; Ruebusch, D. J.; Wu, M.; Javey, A. Ordered Arrays of Dual-Diameter Nanopillars for Maximized Optical Absorption. *Nano Lett.* **2010**, *10*, 3823-3827.

(16) Huang, C. Y.; Wang, D. Y.; Wang, C. H.; Chen, Y. T.; Wang, Y. T.; Jiang, Y. T.; Yang, Y. J.; Chen, C. C.; Chen, Y. F. Efficient Light Harvesting by Photon Downconversion and Light Trapping in Hybrid ZnS Nanoparticles/Si Nanotips Solar Cells. *ACS Nano* **2010**, *4*, 5849-5854.

(17) Chang, H. C.; Lai, K. Y.; Dai, Y. A.; Wang, H. H.; Lin, C. A.; He, J. H. Nanowire Arrays with Controlled Structure Profile for Maximizing Optical Collection Efficiency. *Energy Environ. Sci.* **2011**, *4*, 2863-2869.

(18) Zhao, L.; Lin, Z. Crafting Semiconductor Organic-Inorganic Nanocomposites via Placing Conjugated Polymers in Intimate Contact with Nanocrystals for Hybrid Solar Cells. *Adv. Mater.* **2012**, *24*, 4353-4368.

(19) Wang, H. P.; Lin, T. Y.; Tsai, M. L.; Tu, W. C.; Huang, M. Y.; Liu, C. W.; Chueh, Y. L.; He, J. H. Toward Efficient and Omnidirectional N-type Si Solar Cells: Concurrent Improvement in Optical and Electrical Characteristics by Employing Microscale Hierarchical Structures. *ACS Nano* **2014**, *8*, 2659-2669.

(20) *$1/W Photovoltaic Systems*; U.S. Department of Energy, Washionton, DC, 2010.

(21) Tang, L.; Ji, R.; Cao, X.; Lin, J.; Jiang, H.; Li, X.; Teng, K. S.; Luk, C. M.; Zeng, S.; Hao, J.; Lau, S. P. Deep Ultraviolet Photoluminescence of Water-Soluble Self-Passivated Graphene Quantum Dots. *ACS Nano* **2012**, *6*, 5102-5110.

(22) Kim, J. K.; Park, M. J.; Kim, S. J.; Wang, D. H.; Cho, S. P.; Bae, S.; Park J. H.; Hong, B. H. Balancing Light Absorptivity and Carrier Conductivity of Graphene Quantum Dots for High-Efficiency Bulk Heterojunction Solar Cells. *ACS Nano* **2013**, *7*, 7207-7212.

(23) Shockley, W.; Queisser, H. J. Detailed Balance Limit of Efficiency of p-n Junction Solar Cells. *J. Appl. Phys.* **1961**, *32*, 510-519.

(24) Oshima, C.; Nagashima, A. Ultra-Thin Epitaxial Films of Graphite and Hexagonal Boron Nitride on Solid Surfaces. *J. Phys.: Condens. Matter* **1997**, *9*, 1-20.

(25) Sze, S. M.; Ng, K. K. Physics of Semiconductor Devices. Wiley-interscience: 2006.

(26) Zhang, Y.; Zn, F.; Lee, S. T.; Liao, L.; Zhao, N.; Sun, B. Heterojunction with Organic Thin Layers on Silicon for Record Efficiency Hybrid Solar Cells. *Adv. Energy Mater.* **2014**, *4*, doi: 10.1002/aenm.201300923.